Quantum charge pumping through resonant crossed Andreev reflection in a superconducting hybrid junction of silicene

Ganesh C. Paul and Arijit Saha

Institute of Physics, Sachivalaya Marg, Bhubaneswar, Orissa, 751005, India
and Homi Bhabha National Institute, Training School Complex, Anushakti Nagar, Mumbai 400085, India

We theoretically investigate the phenomena of adiabatic quantum charge pumping through a normal-insulator-superconductor-insulator-normal (NISIN) setup of silicene within the scattering matrix formalism. Assuming a thin barrier limit, we consider the strength of the two barriers (χ_1 and χ_2) as the two pumping parameters in the adiabatic regime. Within this geometry, we obtain crossed Andreev reflection (CAR) with probability unity in the χ_1-χ_2 plane without concomitant transmission or elastic co-tunneling. Tunability of the band gap at the Dirac point by applying an external electric field perpendicular to the silicene sheet and variation of the chemical potential at the normal silicene region, open up the possibility of achieving either a perfect CAR or transmission process through our setup. This resonant behavior is periodic with the barrier strengths. We analyze the behavior of the pumped charge through the NISIN structure as a function of the pumping strength and angles of the incident electrons. We show that large ($Q \sim 2e$) pumped charge can be obtained through our geometry when the pumping contour encloses either the CAR or transmission resonance in the pumping parameter space. We discuss possible experimental feasibility of our theoretical predictions.

I. INTRODUCTION

In recent years, a close cousin to graphene [1,2], silicene [3–11] consisting of a monolayer honeycomb structure of silicon atoms, has attracted a lot of research interest in the condensed matter community due to its unique Dirac-like band structure which allows one to realize a rich variety of topological phases [12–17] and Majorana fermion [16] in it under suitable circumstances. Moreover, this band structure is shown to be tunable by an external electric field applied perpendicular to the silicene sheet [18,19]. Dirac fermions, in turn, become massive at the two valleys **K** and **K**′ in this material. These properties have enabled silicene to be a promising candidate for realizing spintronics [20–24], valleytronics [14,25–27] devices, as well as a silicon-based transistor [28] at room temperature.

Very recently, the superconducting proximity effect in silicene has been investigated theoretically in Refs. [29–31]. Although, up to now, no experiment has been put forwarded in the context of proximity effect in silicene. In Ref. [29], a unique possibility of acquiring pure crossed Andreev reflection (CAR) without any contamination from normal transmission/co-tunneling (CT) has been reported in normal-superconductor-normal (NSN) junction of silicene where elastic co-tunneling as well as Andreev reflection can be suppressed to zero by properly tuning the chemical potential and band gap at the two normal sides. However, in such an NSN junction, the maximum value of CAR probability does not reach 100% because normal reflection does not vanish. This naturally motivates us to study an NISIN junction of silicene and explore whether incorporating an insulating barrier at each NS interface can give rise to resonant CAR in such a setup.

On the other hand, adiabatic quantum pumping is a transport phenomenon in which low-frequency periodic modulations of at least two system parameters [32–35] with a phase difference lead to a zero bias finite dc current in meso- and nanoscale systems. Such zero-bias current is obtained as a consequence of the time variation of the parameters of the quantum system,

which explicitly breaks time-reversal symmetry [36–38]. It is necessary to break time-reversal symmetry in order to get net pumped charge, but it is not a sufficient condition. Indeed, in order to obtain a finite net pumped charge, parity or spatial symmetry must also be broken. Finally, to reach the adiabatic limit, the required condition to satisfy is that the period T of the oscillatory driving signals has to be much larger than the dwell time $\tau_{\text{dwell}} \simeq L/v_F$ of the electrons inside the scattering region of length L, i.e., $T = 2\pi/\omega \gg \tau_{\text{dwell}}$ [34]. In this limit, the pumped charge in a unit cycle becomes independent of the pumping frequency. This is referred to as "adiabatic quantum charge pumping" [34].

During the past decades, quantum charge and spin pumping has been studied extensively in mesoscopic setups including quantum dots and quantum wires both at the theoretical [36,37,39,39–53] as well as experimental [54–59] level with focus on both the adiabatic and nonadiabatic regime. In recent times, quantum pumping has been explored in Dirac systems like graphene [38,50,51,60,61] and topological insulator [62,63]. However, the possible quantization of pumped charge [64] during a cycle through noninteracting open quantum systems has been investigated so far based on the resonant transmission process [38,43,65,66]. In more recent times, quantized behavior of pumped charge has been predicted in superconducting wires with Majorana fermions [67], fractional fermions [66], and topological insulators in enlarged parameter spaces [68]. Although, to date, quantum pumping phenomena through the resonant CAR process has not been investigated to the best of our knowledge.

Motivated by the above mentioned facts, in this article, we study adiabatic quantum charge pumping either through the resonant CAR process or the resonant transmission process, under suitable circumstances, in the silicene NISIN junction. We model our pump setup within the scattering matrix formalism [33,34] and consider the strength of the two barriers (in the thin barrier limit) as our pumping parameters. We show that CAR probability can be unity in the pumping parameter
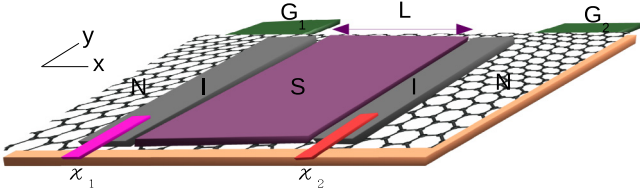
FIG. 1. A schematic sketch of our silicene NISIN setup. A silicene sheet with hexagonal lattice structure is deposited on a substrate (orange, light gray). Here N indicates the normal region, I denotes the thin insulating barrier region (gray, light gray). A bulk superconducting material of length L, denoted by S (pink, light gray), is placed in close proximity to the silicene sheet to induce a superconducting correlation in it. Two gates G_1 and G_2 (dark green, dark gray) are connected to the two normal regions (N) of the silicene sheet to tune the chemical potential (doping) there. Two extra gates (blue and red, light gray) indicated by χ_1 and χ_2 are symbolically denoted to modulate the barrier strengths.

space. Moreover, resonant CAR is periodic in the pumping parameter space due to the relativistic nature of the Dirac fermions. Similar periodicity is present, in the case of the resonant tunneling process as well, under suitable conditions. Adiabatic quantum pumping through these processes, with the modulation of two barrier strengths, can lead to large pumped charge from one reservoir to the other. We investigate the nature of pumped charge through the NISIN structure as a function of the pumping strength and angle of incidence of incoming electrons choosing different types of pumping contours (circular, elliptic, lemniscate [66], etc.).

The remainder of the paper is organized as follows. In Sec. II, we describe our pump setup based on the silicene NISIN junction and the formula for computing pumped charge within the scattering matrix framework. Section III is devoted to the numerical results obtained for the pumped charge as a function of various parameters of the systems. Finally, we summarize our results and conclude in Sec. IV.

II. MODEL AND METHOD

In this section we describe our pump setup in which we consider a normal-insulator-superconductor-insulator-normal (NISIN) structure of silicene in the x-y plane as depicted in Fig. 1. Here, the superconducting region being located between $0 < x < L$, while the insulating barriers are situated on its left, $-d < x < 0$, and on its right, $L < x < L + d$. The normal region of silicene occupies at the extreme left, i.e., $x < -d$ and extreme right ends, $x > L + d$. Here, superconductivity is assumed to be induced in the silicene sheet via the proximity effect, where a bulk s-wave superconductor is placed in close proximity to the sheet in the region $0 < x < L$. The two insulating regions in silicene have gate tunable barriers of strength χ_1 and χ_2 in the thin barrier limit [30,31]. Two additional gate voltages G_1 and G_2 can tune the chemical potential in the left and right normal silicene regions, respectively.

The silicene NISIN junction can be described by the Dirac Bogoliubov–de Gennes (DBdG) equation of the form [29,30],

$$\begin{bmatrix} \hat{H}_{\tilde{\eta}} & \Delta\hat{1} \\ \Delta^\dagger\hat{1} & -\hat{H}_{\tilde{\eta}} \end{bmatrix}\Psi = E\Psi, \quad (1)$$

where E is the excitation energy, and Δ is the proximity induced superconducting pairing gap. The Hamiltonian $H_{\tilde{\eta}}$ describes the low energy physics close to each $\mathbf{K}$ and $\mathbf{K}'$ Dirac points and reads as [19]

$$H_{\tilde{\eta}} = \hbar v_f(\tilde{\eta}k_x\hat{\tau}_x - k_y\hat{\tau}_y) + (elE_z - \tilde{\eta}\sigma\lambda_{\mathrm{SO}})\hat{\tau}_z - \mu\hat{1}, \quad (2)$$

where v_f is the Fermi velocity of the electrons, μ is the chemical potential, λ_{SO} is the spin-orbit term and E_z is the external electric field applied perpendicular to the silicene sheet. Here $\tilde{\eta} = \pm 1$ denotes the $\mathbf{K}$ and $\mathbf{K}'$ valley. In Eq. (2), σ is the spin index and $\hat{\tau}$ correspond to the Pauli matrices acting on the sublattices A and B where $\hat{1}$ is the 2×2 identity operator.

The potential energy term elE_z in the low energy Hamiltonian $H_{\tilde{\eta}}$ originates due to the buckled structure of silicene in which the A and B sublattices are noncoplanar (separated by a distance of length l) and therefore acquire a potential difference when an external electric field E_z is applied perpendicular to the plane. It turns out that at a critical electric field $E_z^c = \lambda_{\mathrm{SO}}/el$, the band gap at each of the valleys become zero with the gapless modes of one of the valley being up-spin polarized and the other being down-spin polarized [18,19]. Away from the critical field, the bands (corresponding to $H_{\tilde{\eta}}$) at each of the valleys $\mathbf{K}$ and $\mathbf{K}'$ split into two conduction and valence bands with the band gap being $|elE_z - \tilde{\eta}\sigma\lambda_{\mathrm{SO}}|$. Note that, in silicene, the pairing occurs between $\tilde{\eta} = 1, \sigma = 1$ and $\tilde{\eta} = -1, \sigma = -1$ as well as $\tilde{\eta} = 1, \sigma = -1$ and $\tilde{\eta} = -1, \sigma = 1$ for an s-wave superconductor.

Here we set up the equations to analyze the quantum pumping phenomena through our NISIN structure. Solving Eq. (1) we find the wave functions in three different regions. The wave functions for the electrons (e) and holes (h) moving in the $\pm x$ direction in the left or right normal silicene region N reads

$$\psi_{Nm}^{e\pm} = \frac{1}{A}\begin{bmatrix} \frac{\pm\tilde{\eta}k_{1m}^e e^{\pm i\tilde{\eta}\alpha_{em}}}{\tau_{1m}^e} \\ 1 \\ 0 \\ 0 \end{bmatrix} \exp\left[i\left(\pm k_{1_{x}m}^e x + k_{1_y}^e y\right)\right],$$

$$(3)$$

$$\psi_{Nm}^{h\pm} = \frac{1}{B}\begin{bmatrix} 0 \\ 0 \\ \frac{\pm\tilde{\eta}k_{1m}^h e^{\pm i\tilde{\eta}\alpha_{hm}}}{\tau_{1m}^h} \\ 1 \end{bmatrix} \exp\left[i\left(\pm k_{1_{x}m}^h x + k_{1_y}^h y\right)\right],$$

where the index $m = \mathrm{L/R}$ stands for the left or right normal silicene region and we use this symbol for the rest of the paper. In Eq. (3) the normalization factors are given by $A = \sqrt{\frac{2(E+\mu_m)}{\tau_{1m}^e}}$, $B = \sqrt{\frac{2(E-\mu_m)}{\tau_{1m}^h}}$, and

$$k_{1m}^{e(h)} = \sqrt{\left(k_{1_{x}m}^{e(h)}\right)^2 + \left(k_{1_y}^{e(h)}\right)^2}, \quad (4)$$

$$k_{1_{x}m}^{e(h)} = \sqrt{(E\pm\mu_m)^2 - (elE_{zm} - \tilde{\eta}\sigma\lambda_{\mathrm{SO}})^2 - \left(k_{1_y}^{e(h)}\right)^2}, \quad (5)$$

$$\tau_{1m}^{e(h)} = E\pm\mu_m\mp(elE_{zm} - \tilde{\eta}\sigma\lambda_{\mathrm{SO}}). \quad (6)$$

Here μ_m indicates the chemical potential in the left (μ_L) or right (μ_R) normal silicene region. E is the energy of the incident particle.

Due to the translational invariance in the y direction, corresponding momentum $k_{1_y}^{e(h)}$ is conserved. Hence, the angle of incidence α_{em} and the Andreev reflection (AR) angle α_{hm}

are related via the relation,

$$k_{1m}^h \sin(\alpha_{hm}) = k_{1m}^e \sin(\alpha_{em}). \tag{7}$$

In the insulating region I, the corresponding wave functions can be inferred from normal region wave functions [Eq. (3)] by replacing $\mu_m \to \mu_m - V_0(V_0')$ where V_0 and V_0' are the applied gate voltages at the left and right insulating regions, respectively. We define dimensionless barrier strengths [30,31] $\chi_1 = V_0 d/\hbar v_F$ and $\chi_2 = V_0' d/\hbar v_F$ which we use as pumping parameters for our analysis. Here d is the width of the insulating barriers assumed to be the same for both of them.

In the superconducting region S, the wave functions of DBdG quasiparticles are given by

$$\psi_S^{e\pm} = \frac{1}{\sqrt{2}} \begin{bmatrix} u_1 \\ \pm\tilde{\eta} u_1 e^{i\tilde{\eta}\theta_e} \\ u_2 \\ \pm\tilde{\eta} u_2 e^{i\tilde{\eta}\theta_e} \end{bmatrix} \exp[\pm(i\mu_S - \kappa)x + iq_y^e y],$$

$$\psi_S^{h\mp} = \frac{1}{\sqrt{2}} \begin{bmatrix} u_2 \\ \mp\tilde{\eta} u_2 e^{-i\tilde{\eta}\theta_h} \\ u_1 \\ \mp\tilde{\eta} u_1 e^{-i\tilde{\eta}\theta_e} \end{bmatrix} \exp[\pm(-i\mu_S - \kappa)x + iq_y^h y].$$
$$\tag{8}$$

Here the coherence factors are given by

$$u_{1(2)} = \left[\frac{1}{2} \pm \frac{\sqrt{E^2 - \Delta^2}}{2E}\right]^{\frac{1}{2}} \text{ and } \kappa = \sqrt{\Delta^2 - E^2}. \tag{9}$$

As before, the translational invariance along the y direction relates the transmission angles for the electronlike and holelike quasiparticles via the following relation given by

$$q^\beta \sin\theta_\beta = k_{1m}^e \sin\alpha_{em}, \tag{10}$$

for $\beta = e,h$. The quasiparticle momentum can be written as

$$q^{e(h)} = \mu_S \pm \sqrt{E^2 - \Delta^2}, \tag{11}$$

where $\mu_S = \mu_m + U_0$, and U_0 is the gate potential applied to the superconducting region in order to tune the Fermi wavelength mismatch [69] between the normal and superconducting regions. The requirement for the mean-field treatment of superconductivity is justified in our model as we have taken $\mu_S \gg \Delta$ [69,70] throughout our calculation.

We consider electrons with energy E incident from the left normal region of the silicene sheet in the subgapped regime ($E < \Delta$). Considering normal reflection, Andreev reflection, co-tunneling (normal transmission), and crossed Andreev reflection from the interface, we can write the wave functions in five different regions of the junction as

$$\Psi_N^L = \psi_{NL}^{e+} + r_e \psi_{NL}^{e-} + r_A \psi_{NL}^{h-},$$
$$\Psi_I^L = p_1 \psi_{IL}^{e+} + q_1 \psi_{IL}^{e-} + m_1 \psi_{IL}^{h+} + n_1 \psi_{IL}^{h-},$$
$$\Psi_S = t_1 \psi_S^{e+} + t_2 \psi_S^{e-} + t_3 \psi_S^{h+} + t_4 \psi_S^{h-}, \tag{12}$$
$$\Psi_I^R = p_2 \psi_{IR}^{e+} + q_2 \psi_{IR}^{e-} + m_2 \psi_{IR}^{h+} + n_2 \psi_{IR}^{h-},$$
$$\Psi_N^R = t_e \psi_{NR}^{e+} + t_A \psi_{NR}^{h+},$$

where r_e, r_A, t_e, t_A correspond to the amplitudes of normal reflection, AR, transmission, and CAR in the N silicene regions, respectively. The transmission amplitudes t_1, t_2, t_3, and t_4 denote the electronlike and holelike quasiparticles in the

S region. Using the boundary conditions at the four interfaces, we can write

$$\Psi_N^L|_{x=-d} = \Psi_I^L|_{x=-d}, \quad \Psi_I^L|_{x=0} = \Psi_S|_{x=0},$$
$$\Psi_S|_{x=L} = \Psi_I^R|_{x=L}, \quad \Psi_I^R|_{x=L+d} = \Psi_N^R|_{x=L+d}, \tag{13}$$

which yields a set of 16 linearly independent equations. Solving these equations numerically, we obtain r_e, r_A, t_e, t_A which are required for the computation of pumped charge through our setup.

In order to carry out our analysis for the pumped charge in silicene NISIN structure, we choose the two dimensionless insulating barrier strengths χ_1 and χ_2 as our pumping parameters. They evolve in time either as (offset circular contours)

$$\chi_1 = \chi_0 + P\cos(\omega t - \eta),$$
$$\chi_2 = \chi_0 + P\cos(\omega t + \eta), \tag{14}$$

or as ("lemniscate" contours),

$$\chi_1 = \chi_{1_0} + P_L\left(\cos\theta\cos\omega t - \tfrac{1}{2}\sin\theta\sin 2\omega t\right)/(1 + \sin^2\omega t),$$
$$\chi_2 = \chi_{2_0} + P_L\left(\cos\theta\cos\omega t + \tfrac{1}{2}\sin\theta\sin 2\omega t\right)/(1 + \sin^2\omega t), \tag{15}$$

respectively. In the circular contours χ_0 and in the lemniscate contours χ_{1_0}, χ_{2_0} correspond to the mean value of the amplitude, respectively, around which the two pumping parameters are modulated with time. P and P_L are called the pumping strengths for the two types of contours, respectively. Furthermore, 2η and θ represent the phase offset between the two pumping signals for the circular and lemniscate contours, respectively. Here ω is the frequency of oscillation of the pumping parameters.

We, in our analysis, only consider the adiabatic limit of quantum pumping where the time period of the pumping parameters $T = 2\pi/\omega$ is much longer than the dwell time $\tau_{\text{dwell}} \simeq L/v_F$ of the Dirac fermions inside the proximity induced superconducting region.

To calculate the pumped charge, we employ Brouwer's formula [34] which relies on the knowledge of the parametric derivatives of the S-matrix elements. Following Ref. [71], the S matrix for the NISIN structure of silicene for an incident electron with energy E, can be written as

$$S = \begin{bmatrix} |r_e|e^{i\gamma_e} & |r_A|e^{i\gamma_h} & |t_e|e^{i\delta_e} & |t_A|e^{i\delta_h} \\ |r_A|e^{i\gamma_h} & |r_e|e^{i\gamma_e} & |t_A|e^{i\delta_h} & |t_e|e^{i\delta_e} \\ |t_e|e^{i\delta_e} & |t_A|e^{i\delta_h} & |r_e|e^{i\gamma_e} & |r_A|e^{i\gamma_h} \\ |t_A|e^{i\delta_h} & |t_e|e^{i\delta_e} & |r_A|e^{i\gamma_h} & |r_e|e^{i\gamma_e} \end{bmatrix}. \tag{16}$$

We write here the complex S-matrix elements S_{ij} in polar form, with modulus and phase explicitly shown, since the phase is going to play a major role in the determination of the pumped charge. For a single channel S matrix, the formula for the pumped charge becomes [71]

$$Q = \frac{e}{2\pi} \int_0^T dt[-|r_A|^2(\dot{\gamma}_h \cos\alpha_{hL} + \dot{\gamma}_e \cos\alpha_{eL})$$
$$- |t_A|^2(\dot{\delta}_h \cos\alpha_{hR} + \dot{\gamma}_e \cos\alpha_{eL})$$
$$+ |t_e|^2(\dot{\delta}_e \cos\alpha_{eR} - \dot{\gamma}_e \cos\alpha_{eL}) + \dot{\gamma}_e \cos\alpha_{eL}]. \tag{17}$$

Here, we have redefined the complex scattering amplitudes r_A and t_A to satisfy the conservation of probability current [29]. On the other hand, the other two scattering amplitudes r_e and t_e remain unchanged. Hence, the redefined scattering probabilities $|r_A|^2$ and $|t_A|^2$ become

$$|r_A|^2 \equiv \frac{k_{1_x}^h}{k_{1_x}^e} \left[\frac{2(E + \mu_L)(E - \mu_L - \lambda_L)}{|\eta k_{1_x}^h - i k_{1_y}^e|^2 + (E - \mu_L - \lambda_L)^2} \right] |r_A|^2,$$

$$|t_A|^2 \equiv \frac{k_{1_x}^h}{k_{1_x}^e} \left[\frac{(E + \mu_L)}{(E - \mu_R)} \right] |t_A|^2. \qquad (18)$$

Furthermore, γ_e, γ_h, δ_e, δ_h are the phases of redefined r_e, r_A, t_e, and t_A, respectively. Here, α_{eL}, α_{eR} correspond to the incident and transmitted angles of electrons while α_{hL}, α_{hR} represent the reflected and transmitted angles of holes, respectively. Note that, if $\alpha_{eL} = 0$, then the last term of Eq. (17) consisting of the time derivative of reflection phase is called "*topological part*" [46] while the rest is termed as "*dissipative part*" [46]. The last term is called "topological" because for $\alpha_{eL} = 0$, it has to return to itself after the full period. Hence, the only possible change in γ_e in a period can be integer multiples of 2π, i.e., $\gamma_e(T) \rightarrow \gamma_e(0) + 2\pi n$. On the other hand, the rest of the terms in Eq. (17) are together called "dissipative" since their cumulative contribution prevents the perfect quantization of pumped charge.

III. NUMERICAL RESULTS

In this section we present and discuss our numerical results for the pumped charge based on Eq. (17). The quantum mechanical scattering amplitudes are all functions of the incident electron energy E, length of the superconducting silicene region L, the strengths χ_1, χ_2 of the two thin insulating barriers, chemical potential μ_m ($m = $ L/R) of the left and right normal silicene region, external electric field E_{zm} ($m = $ L/R), and spin-orbit coupling λ_{SO}. We denote the band gaps at the left and right normal silicene side as $2\lambda_L$ and $2\lambda_R$, respectively (see Fig. 2), where $\lambda_m = (el E_{zm} - \tilde{\eta}\sigma\lambda_{SO})$. In addition, we have set $\hbar = 1$ throughout our analysis.

For clarity, we divide this section into two subsections. In the first one, we discuss quantum pumping via the resonant CAR process with unit probability in the χ_1-χ_2 plane. The corresponding results are demonstrated in Figs. 3–7. The second one is devoted to the discussion of the same via the perfect transmission/CT process. We present the corresponding results in Figs. 8–12.

A. Pumping via CAR in the χ_1-χ_2 plane

Silicene is a material where a large value of the nonlocal CAR process can be obtained due to its unique band structure [29]. The band gaps and Fermi level (chemical potential) in silicene can be tuned by applying electric fields only. By tuning the both, very recently, Linder *et al.* in Ref. [29] showed that one can completely block elastic co-tunneling in the silicene NSN junction in the subgapped regime. Consequently, the pure CAR process is possible for a broad range of energies. However, maximum probability of CAR found in Ref. [29] was ~96.2% while the rest was normal reflection probability.
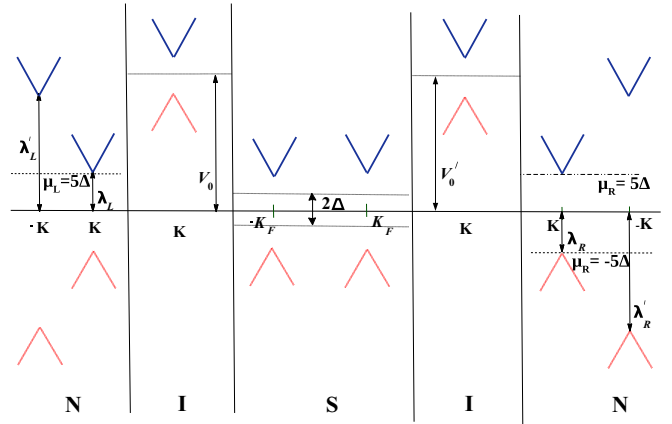

FIG. 2. A schematic sketch of the band structure of our silicene NISIN setup is depicted. For the normal regions of silicene (N) as well as superconducting (S) silicene region, both **K** and **K**′ valleys are presented. In contrast, only the **K** valley is shown for both the insulating regions (I) for simplicity. Blue solid line indicates the conduction band while the valence bands are represented by red solid lines. At the right normal silicene side, the chemical potential is set at the top of the valance band ($\mu_R = -5\Delta$, dotted line) to obtain the resonant CAR process. On the other hand, for resonant transmission to take place, chemical potential in the right normal side is set at the bottom of the conduction band ($\mu_R = 5\Delta$, dot-dashed line).

The probability of the nonlocal CAR process can be enhanced to unity (100%) (see Fig. 4) by introducing two insulating barriers at each NS interfaces. We have considered $\mu_L = 5\Delta$, $\mu_R = -5\Delta$, and $\lambda_L = \lambda_R = 5\Delta$, which reflects the fact that the Fermi level touches the bottom of the conduction band in the left normal silicene side while it touches the top of the valence band in the right normal silicene side. This is illustrated in Fig. 2. The superconducting silicene side is doped with $\mu_S = 20\Delta$ to satisfy mean-field condition for superconductivity $\mu_S \gg \Delta$ [29]. The band gaps λ_L and λ_R at the two normal sides can be adjusted by the external electric field E_{zm} ($m = $ L/R). The chosen value of the band gaps and doping levels permits one to neglect the contribution from the
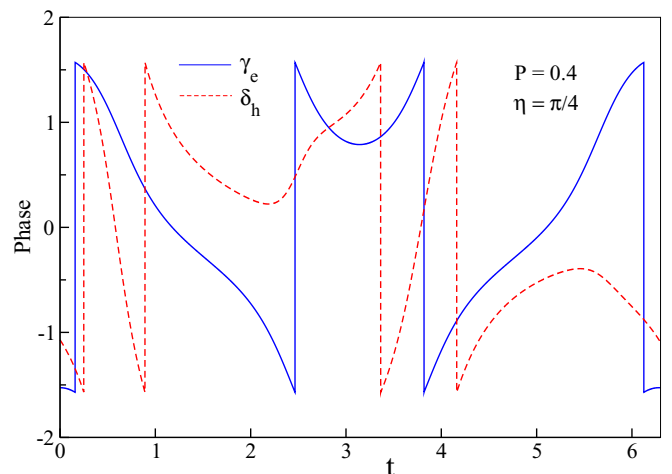

FIG. 3. The plot shows the variation of the normal reflection phase γ_e and CAR phase δ_h, with time t, along a chosen pumping contour in the χ_1-χ_2 plane.

other valley ($\mathbf{K}'$) which has a much higher band gap compared to the other energy scales in the system (see Fig. 2). Under such circumstances, we obtain pure CAR in this setup choosing length of the superconducting side, $L = 2.1\xi$ ($\xi = \hbar v_F / \pi \Delta$ is the phase coherence length of the superconductor) and incident electron energy, $E = 0.9\Delta$. Note that, for our analysis, we choose the same parameter values as used in Ref. [29].

The reason behind obtaining the pure CAR process in our NISIN setup is as follows. As there is a band gap $2\lambda_L = 2(elE_{zL} - \tilde{\eta}\sigma\lambda_{\rm SO}) > \Delta$ in the left normal silicene side, probability for AR to take place is vanishingly small [29,31]. On the other hand, $2\lambda_R = 2(elE_{zR} - \tilde{\eta}\sigma\lambda_{\rm SO})$ is the energy gap between the conduction band and valance band in the right (R) normal silicene region as illustrated in Fig. 2. Moreover, the chemical potential μ_R in the right (R) normal silicene is chosen to be at the top of the valence band. Hence, only hole states are available in the right normal side. Therefore, an electron incident from the conduction band of the left normal silicene region encounters a gap and unavailability of electronic states to tunnel into the right normal region which essentially block the co-tunneling probability. Hence, the only possible scattering processes remaining are normal reflection and CAR. This allows our system to possess completely the pure CAR process with probability one in the χ_1-χ_2 plane as shown in Fig. 4. These resonant CAR peaks are $\pi/2$ periodic in nature and they appear in pairs. Such a periodic nature, and the fact that resonances appear in pairs, affect the pumped charge behavior which will be discussed later. The oscillatory behavior of the CAR resonance can be explained as follows. Nonrelativistic free electrons with energy E incident on a potential barrier with height V_0 are described by an exponentially decaying (nonoscillatory) wave function inside the barrier region if $E < V_0$, since the dispersion relation is $k \sim \sqrt{E - V_0}$. On the contrary, relativistic free electrons satisfies a dispersion $k \sim (E - V_0)$, consequently corresponding wave functions do not decay inside the barrier region [30,72,73]. Instead, the transmittance of the junction displays an oscillatory behavior as a function of the strength of the barrier. Hence, the undamped oscillatory behavior of CAR is a direct manifestation of the relativistic low-energy Dirac fermions in silicene. The periodicity depends on the Fermi wavelength mismatch between the normal and superconducting region [30,31].

Note that the Fermi energy (chemical potential) does not need to necessarily exactly touch valance band maxima or conduction band minima nor does it need to have the same magnitude at the two normal regions to obtain resonant CAR. A small deviation, from the numerical values that we have taken, also leads to the resonant CAR probability to take place within the subgapped regime. Previously, the possibility of obtaining CAR was also reported in the *p*-*n* junction of graphene [74] at a specific value of the parameters. However, a small deviation from that leads to CT along with CAR contaminating that possibility.

As phases of the scattering amplitudes play a major role in the determination of the pumped charge, we show the behavior of phases of normal reflection and CAR amplitudes (γ_e and δ_h, respectively) as a function of time for one full cycle in Fig. 3. We observe that both γ_e and δ_h exhibit four abrupt jumps for a full period of time (along a chosen contour). These
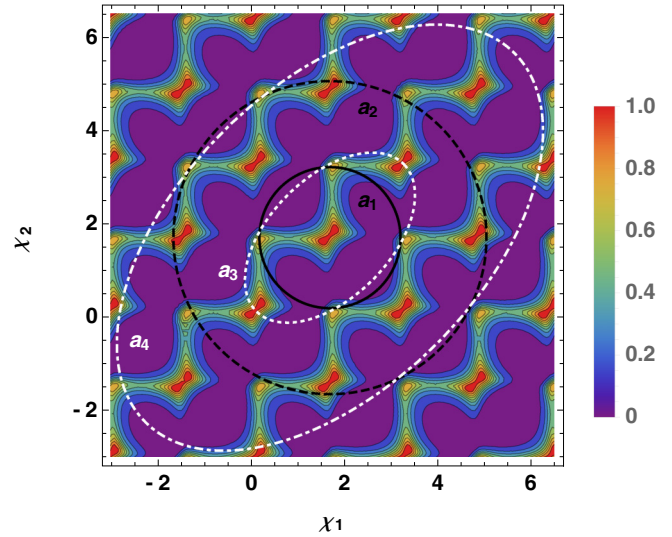

FIG. 4. Plot of CAR probability $|t_A|^2$ in the χ_1-χ_2 plane. The contours a_1, a_2 represent $\eta = \pi/4$ and $P = 1.51$, $P = 3.35$, respectively. On the other hand, the contours a_3, a_4 are for $\eta = \pi/6$ and $P = 1.82$, $P = 4.56$, respectively. The value of the other parameters are chosen to be $L = 2.1\xi$, $E = 0.9\Delta$, $\omega = 1$, $\chi_0 = 1.7$, $\mu_L = 5\Delta$, $\mu_R = -5\Delta$, $\mu_S = 20\Delta$, and $\lambda_L = \lambda_R = 5\Delta$.

jumps play a significant role in determining the pumped charge which we emphasize later. In addition, throughout our analysis, we have considered incident electrons to be normal to the interface, i.e., $\alpha_{eL} = 0$ for simplicity. Later for completeness, we demonstrate angle dependence of the pumped charge.

Under such a scenario where the only possible scattering processes are normal reflection and CAR, Eq. (17) simplifies to

$$Q = \frac{e}{2\pi} \int_0^T dt [-|t_A|^2 (\dot{\delta}_h \cos\alpha_{hR} + \dot{\gamma}_e \cos\alpha_{eL}) + \dot{\gamma}_e \cos\alpha_{eL}]. \tag{19}$$

The behavior of pumped charge Q as a function of the pumping strength P is shown in Fig. 5 for $\eta = \pi/4, \pi/6$ which correspond to circular and elliptic contours, respectively. The features of Q, depicted in Fig. 5, can be understood from the behavior of CAR probability $|t_A|^2$ in the χ_1-χ_2 plane. For small values of P, pumped charge Q becomes vanishingly small in magnitude as the pumping contours do not enclose any $|t_A|^2 = 1$ point. When a pumping contour encloses one of the resonant peaks of $|t_A|^2$, the topological part of the pumped charge gives rise to *ne* (*n* is the winding number) due to the integration around a singular point. At this point the reflection phase γ_e becomes ill-defined. However, the dissipative part nullifies the topological part resulting in small values of Q [see Eq. (17)] for both $\eta = \pi/4, \pi/6$. On the other hand, when a contour encloses both $|t_A|^2$ resonances, the relative integration direction around the two singular points plays an important role. Namely, when two resonances are enclosed in a path with the same orientation, then the two contributions have the opposite sign and tend to cancel each other. For example, when $\eta = \pi/4$ (black circular contours a_1 and a_2), the pumped charge is zero for $P = 1.51$ (see Fig. 5) as the contour a_1 encloses both the peaks resulting in zero pumped charge. A
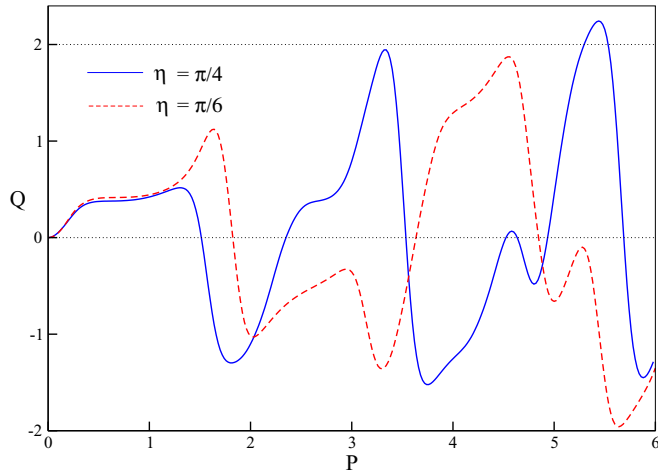
FIG. 5. The pumped charge Q in units of the electron charge e, for pumping in the χ_1-χ_2 plane, is shown as a function of the pumping strength P for circular and elliptic contours. The value of the other parameters are chosen to be the same as mentioned in Fig. 4.

similar feature was found in the case of resonant transmission in Refs. [43,47,65,66] where pumped charge was found to be zero when the pumping contour encloses both the resonances. Q approaches almost quantized value $2e$ for $P = 3.35$ and the corresponding contour a_2 encloses an even number of resonance pairs in the same orientation. Hence the topological part of pumped charge is almost zero and the contribution to Q arises from the dissipative part. The large contribution from the dissipative part arises due to the total drop of the CAR phase δ_h by a factor of 4π during its time evolution along the contour a_2 (see Fig. 3). Similarly, when $\eta = \pi/6$, Q is zero at $P = 1.82$ which corresponds to the a_3 contour which encloses four peaks (two pairs) in total, resulting in zero contribution from the topological part. On the other hand, pumped charge reaches its maximum when $P = 4.56$ (a_4 contour) where also the entire contribution originates from the dissipative part (see Fig. 5). Pumped charge Q exceeds the value $+2e$ as pumping strength P increases (see Fig. 5) for both $\eta = \pi/4$ and $\pi/6$. Physically, the contribution of the dissipative part in pumped charge increases nonmonotonically with the pumping strength. Hence, as the pumping contour encloses more numbers of pairs of resonant CAR peaks, due to the enhancement of the dissipative part, pumped charge can exceed $+2e$ with further increase of P. Pumped charge can change sign depending on the sense of enclosing of the resonances, i.e., whether it is clockwise or anticlockwise.

The behavior of pumped charge Q with respect to the pumping strength P_L for lemniscate contours with $\theta = \pi/4$ and $\pi/3$ is presented in Fig. 7 and the corresponding contours are shown in Fig. 6. The pumped charge is small for small values of P_L where the contribution from the topological part is canceled by the dissipative part. As P_L increases, the corresponding pumping contour encloses both the $|t_A|^2$ peaks within opposite integration orientations and as a consequence, the two contributions for the pumped charge sum up. This is exactly the reason that motivates us to choose the lemniscate contours. However, the dissipative part effectively reduces the total pumped charge. Such a feature arises for lemniscate contours of the type b_1 and b_3. Moreover, we observe that
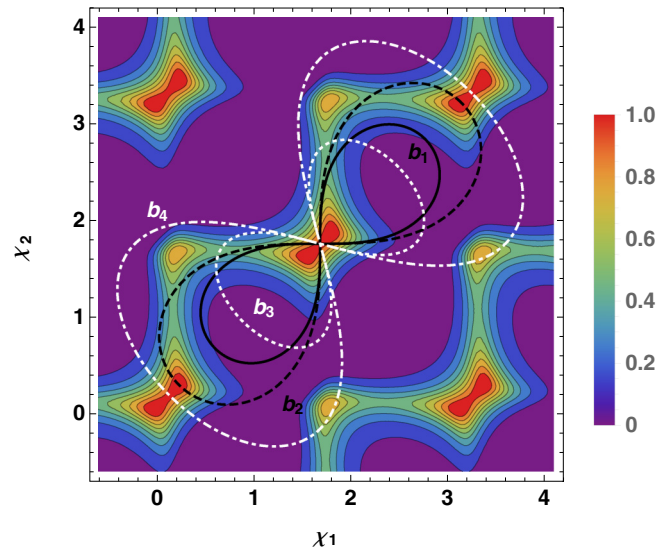

FIG. 6. Plot of CAR probability $|t_A|^2$ along with lemniscate contours are shown in the χ_1-χ_2 plane. The contours b_1, b_2 represent $\theta = \pi/4$ and the contours corresponding to $\theta = \pi/3$ are b_3, b_4. We have chosen the mean values $\chi_{1_0} = 1.69$ and $\chi_{2_0} = 1.75$. The value of the other parameters are chosen to be the same as mentioned in Fig. 4.

the pumped charge becomes zero for $P_L = 2.06$ at $\theta = \pi/4$, where both the bubbles of the b_2 contour enclose two $|t_A|^2$ peaks from the two adjacent resonances in the χ_1-χ_2 plane and hence their combined contribution to pumped charge get canceled for each bubble separately. The qualitative behavior of Q remains similar for $\theta = \pi/3$ where maximum value of Q is achieved when each bubble of the lemniscate contour of type b_4 encloses an odd number of resonance pairs while Q tends to zero as an even number of pairs are enclosed by each bubble of the contour.

B. Pumping via transmission/CT in the χ_1-χ_2 plane

In this subsection we present our numerical results for the adiabatic quantum pumping through pure CT, i.e., resonant
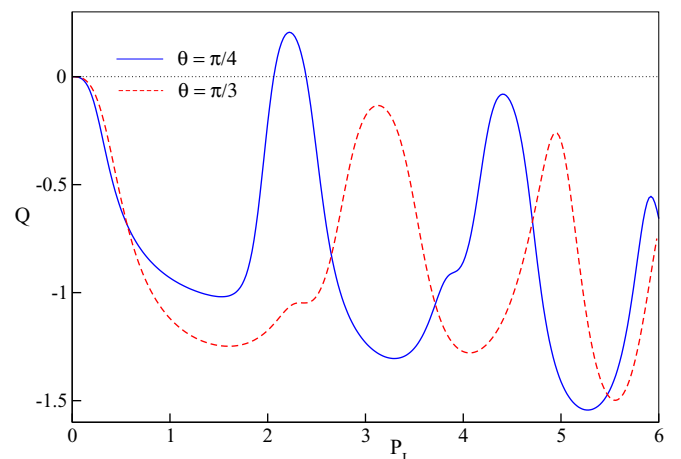

FIG. 7. Pumped charge Q in units of electon charge e, for pumping in the χ_1-χ_2 plane, is shown as a function of the pumping strength P_L for the lemniscate contours. All other parameters are identical to those used in Fig. 4.
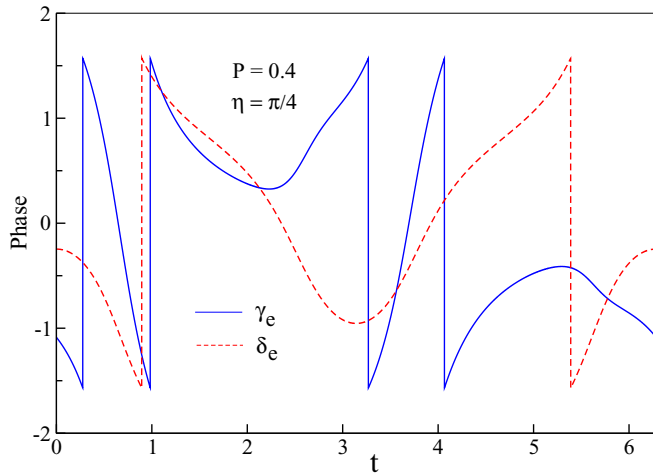
FIG. 8. The variation of the normal reflection phase γ_e and transmission phase δ_e, with time t, is shown along a chosen pumping contour in the χ_1-χ_2 plane.

transmission process. The latter can be achieved by tuning the Fermi level (chemical potential) at the bottom of the conduction band in both the normal silicene regions (see Fig. 2). The numerical values of all the parameters are identical to those used before except now $\mu_R = 5\Delta$, $L = 2.2\,\xi$, and $E = 0.93\Delta$.

As before, due to the presence of a gap ($2\lambda_L > \Delta$) in the left normal side, AR is forbidden while CAR cannot take place because of the unavailability of the hole states in the right normal region in the low-energy limit. An incident electron thus only encounters two scattering processes which are normal reflection and transmission. The presence of insulating barriers between the NS interfaces allows both these scattering probabilities to be oscillatory as a function of the dimensionless barrier strengths χ_1 and χ_2 which is depicted in Fig. 9.

In this regime, as AR and CAR probabilities are always zero, hence Eq. (17) reduces to

$$Q = \frac{e}{2\pi} \int_0^T dt [|t_e|^2 (\dot{\delta}_e \cos\alpha_{eR} - \dot{\gamma}_e \cos\alpha_{eL}) + \dot{\gamma}_e \cos\alpha_{eL}], \quad (20)$$

In Fig. 10, pumped charge Q is presented as a function of pumping strength P for $\eta = \pi/4$ (circular contour) and $\pi/6$ (elliptic contour). To understand the behavior of the pumped charge, we also investigate the transmission probability $|t_e|^2$ in $\chi_1 - \chi_2$ plane (see Fig. 9). We observe qualitatively similar features of the pumped charge as depicted in the previous subsection. Here also the topological part of pumped charge becomes zero when pumping contour encloses an even number of resonance pairs in the same orientation. Finite contribution from the dissipative part, in Q, emerges due to the total jump of the transmission phase δ_e by a factor of 2π during its time evolution along the contour c_2 (see Fig. 8). On the other hand, for contour c_1, the dissipative part vanishes because over a full period of time, reflection, and transmission phases γ_e and δ_e respectively, cancel each other [see Eq. (20)]. Although, Q
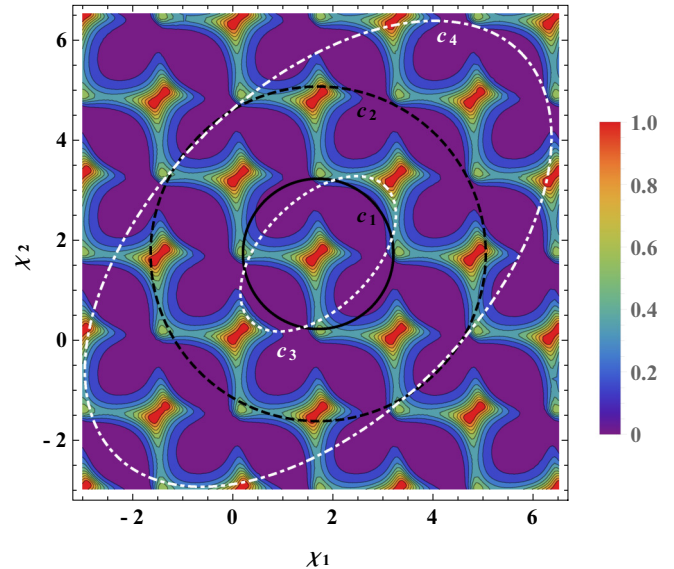

FIG. 9. Transmission probability $|t_e|^2$ along with circular and elliptic contours are shown in the χ_1-χ_2 plane. The contours c_1, c_2 represent $\eta = \pi/4$ and $P = 1.5$, $P = 3.34$, respectively. On the other hand, the contours c_3, c_4 correspond to $\eta = \pi/6$ and $P = 1.55$, $P = 4.65$, respectively. The value of the other parameters are chosen to be $L = 2.2\xi$, $E = 0.93\Delta$, $\omega = 1$, $\chi_0 = 1.7$, $\mu_L = 5\Delta$, $\mu_R = 5\Delta$, $\mu_S = 20\Delta$, and $\lambda_L = \lambda_R = 5\Delta$.

approaches to $-e$ for pumping via the resonant CT process compared to $2e$ via the resonant CAR process.

In Fig. 12, we show the behavior of pumped charge Q as a function of the pumping strength P_L with lemniscate contours. To understand the corresponding behavior of Q, we also show $|t_e|^2$ in the χ_1-χ_2 plane along with different lemniscate contours (see Fig. 11). Here also the features of Q remain similar as the previous subsection for both $\theta = \pi/4$ and $\pi/3$.

As we mention earlier, the above mentioned results are valid for normal incidence of the incoming electron, i.e., $\alpha_{eL} = 0$.
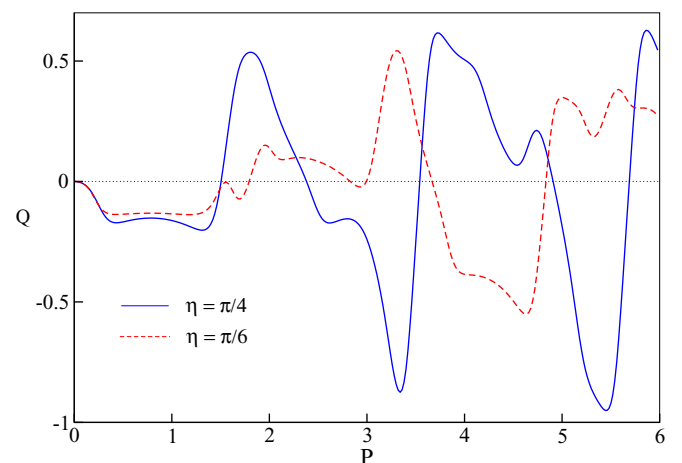

FIG. 10. Pumped charge Q in units of electron charge e, for pumping in the χ_1-χ_2 plane, is shown as a function of the pumping strength P for the circular and elliptic contours. We choose the same values of the other parameters as mentioned in Fig. 9.
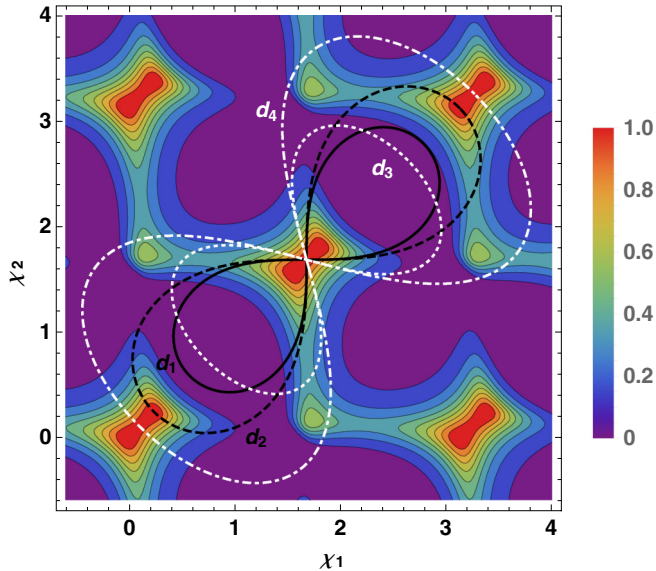
FIG. 11. Transmission probability $|t_e|^2$ together with different lemniscate contours are shown in the χ_1-χ_2 plane. The contours d_1, d_2 represent $\theta = \pi/4$ and the contours d_3, d_4 correspond to $\theta = \pi/3$. We choose the values of χ_{1_0} and χ_{2_0} as $\chi_{1_0} = \chi_{2_0} = 1.68$. All other parameters are identical to those used in Fig. 9.

Here, we explore the dependence of the pumped charge on the angle of incident electrons. In Fig. 13, pumped charge Q as a function of incident angle α_{eL} is presented when either the CAR probability $|t_A|^2$ or transmission probability $|t_e|^2$ is enclosed by the circular pumping contour. The α_{eL} dependence is shown up to the critical angle α_c. Above α_c, the AR and CAR processes cannot take place [69]. Rather, normal reflection is the dominating scattering mechanism above α_c. It is evident from Fig. 13 that as the angle of incidence α_{eL} increases, Q decreases monotonically for enclosing $|t_A|^2$ or $|t_e|^2$ in either cases. The reason can be attributed to the fact that both $|t_A|^2$ and $|t_e|^2$ in the two different scenarios, acquire the maximum value at normal incidence, i.e., $\alpha_{eL} = 0$ and decreases slowly
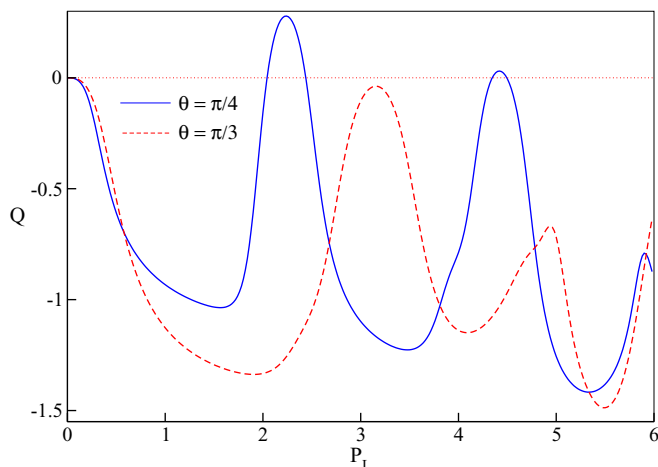

FIG. 12. Pumped charge Q, in units of electron charge e, is depicted as a function of the pumping strength P_L for the lemniscate contours. All other parameters are identical to those used in Fig. 9.
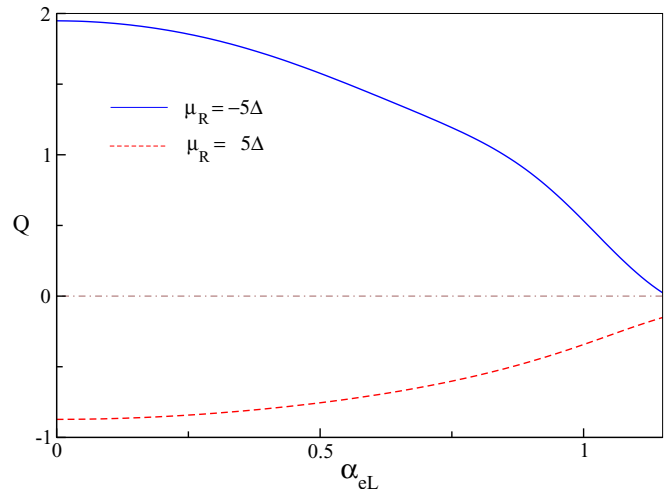

FIG. 13. Pumped charge Q, in units of electron charge e, is shown as a function of the incident angle α_{eL} for both $\mu_R = -5\Delta$ and $\mu_R = 5\Delta$. Here we choose $\eta = \pi/4$, $P = 3.35$ for $\mu_R = -5\Delta$ and $P = 3.34$ for $\mu_R = 5\Delta$, respectively.

with the increase of α_{eL}. Also, for $0 < \alpha_{eL} < \alpha_c$, normal reflection probability $|r_e|^2$ also contributes to Eq. (17) and the interplay between all the quantum mechanical amplitudes and their phases results in a smaller value of pumped charge. Note that, in the case of pumping via the CAR resonance process in the χ_1-χ_2 plane, Q approaches zero as α_{eL} proceeds towards α_c. However, Q is finite even at α_c in the case of pumping via resonant transmission in the same parameter space, This is because at α_c, $|t_A|^2$ vanishes while $|t_e|^2$ still has small probability which gives rise to small pumped charge arising from the dissipative part [see Eq. (20)].

IV. SUMMARY AND CONCLUSIONS

To summarize, in this article, we have investigated the possibility of enhancing the CAR probability $|t_A|^2$ in silicene NSN set up by introducing the thin insulating barrier [30,31] I at each NS interface. We show that, for electrons with normal incidence, resonant CAR can be obtained in our setup by tuning the band gap in both the normal silicene regions by applying an external electric field as well as adjusting the chemical potential by additional gate voltages. We also show that $|t_A|^2$ is periodic in the χ_1-χ_2 plane due to the relativistic nature of Dirac fermions. On the other hand, it is also possible to attain transmission probability $|t_e|^2$ of magnitude unity in the silicene NISIN junction under suitable circumstances. Owing to the Dirac nature of particles, $|t_e|^2$ also exhibits periodic behavior in the space of barrier strengths χ_1 and χ_2.

We then explore adiabatic quantum charge pumping through our NISIN setup and show that the behavior of pumped charge as a function of the pumping strength P is closely related to the features of CAR probability $|t_A|^2$ or transmission probability $|t_e|^2$ in the pumping parameter space. For electrons with normal incidence, large pumped charge with value close to $Q \sim 2e$ can be obtained when particular circular or elliptic pumping contour encloses the resonant CAR in the χ_1-χ_2 plane, although the major contribution to Q, in

this case, arises from the dissipative part. On the other hand, large pumped charge can also be obtained with lemniscate contour when an odd number of $|t_A|^2$ peaks are enclosed by each of their bubbles. In contrast, pumped charge approaches to $Q \sim -e$ when various pumping contours enclose $|t_e|^2$ resonance in the same parameter space. However, pumped charge decreases monotonically as we increase the angle of incidence of the incoming electron. In experimental situations, the measurable quantity should be the angle averaged pumped charge analogous to angle averaged conductance [75]. From our analysis, we expect that the qualitative nature of angle averaged pumped charge as a function of the pumping strength will remain similar to the $\alpha_{eL} = 0$ case. Although the quantitative value of Q will be smaller than the angle resolved case as Q decreases monotonically with α_{eL}.

Note that our calculation is valid for zero temperature. Nevertheless, in our case, temperature T_p must be smaller than the proximity induced superconducting gap Δ. We expect that the qualitative features of our results for the pumped charge will survive in the presence of low temperatures. For nonzero yet small temperatures, $T_p \ll \Delta$, the pairs of resonant peaks in the parameter space will have a slight broadening due to thermal smearing. Therefore, we believe that the qualitative features of pumped charge Q with respect to the pumping strength P will still be captured in our model, although there can be quantitative change in Q. On the other hand, if $T_p > \Delta$, then the CAR process from the interface will decay and pumped charge will become vanishingly small due to thermal fluctuation.

As far as practical realization of our silicene NISIN quantum pumping setup is concerned, superconductivity in silicene may be possible to induce by proximity coupled to an *s*-wave superconductor for, e.g., Al, NbSe$_2$ analogous to graphene [75–77]. Once such proximity induced superconductivity in silicene is realized, fabrication of the silicene NISIN junction can be feasible. The strength of the two oscillating barriers can be possible to tune by applying ac gate voltages. Typical spin-orbit energy in silicene is $\lambda_{SO} \sim 4$ meV and the buckling parameter is $l \approx 0.23$ Å [3,5]. Considering Refs. [76,78], typical proximity induced superconducting gap in silicene would be $\Delta \sim 0.2$ meV. For such an induced superconducting gap, chemical potential is $\mu_S \sim 20\Delta \sim 4$ meV and we obtain $\xi \sim 580$ nm and length of the superconducting region $L \sim 1.2$ μm. Hence, an insulating barrier of thickness $d \sim$ 10–20 nm may be considered as the thin barrier and the gate voltage $V_0 \sim 500$ meV can therefore justify the needs of our model [30]. To achieve both the resonances, $\lambda_L = \lambda_R = 5\Delta \sim 1$ meV which can be tuned by an external electric field $E_{zL} = E_{zR} \sim 200$ V/μm. For both resonant processes, typical dwell time of the electrons inside the superconducting region is ~ 2.2 fs while the time period of the oscillating barriers is $T \sim 30$ ps and the corresponding frequency of modulation parameters turns out to be ~ 230 GHz. Thus the dwell time τ_{dwell} is much smaller than the time period T of the modulation parameters, hence satisfying the adiabatic condition of the quantum pump. Pumped current through our setup should be in the range of ~ 10–15 nA which can be measurable in the modern day experiment.

[1] A. K. Geim and K. S. Novoselov, Nat. Mater. **6**, 183 (2007).

[2] A. H. Castro Neto, F. Guinea, N. M. R. Peres, K. S. Novoselov, and A. K. Geim, Rev. Mod. Phys. **81**, 109 (2009).

[3] C.-C. Liu, H. Jiang, and Y. Yao, Phys. Rev. B **84**, 195430 (2011).

[4] M. Houssa, A. Dimoulas, and A. Molle, J. Phys.: Condens. Matter **27**, 253002 (2015).

[5] M. Ezawa, J. Phys. Soc. Jpn. **84**, 121003 (2015).

[6] A. Hattori, S. Tanaya, K. Yada, M. Araidai, M. Sato, Y. Hatsugai, K. Shiraishi, and Y. Tanaka, arXiv:1604.4717.

[7] T. P. Kaloni, G. Schreckenbach, M. S. Freund, and U. Schwingenschlögl, Phys. Status Solidi RRL **10**, 133 (2016).

[8] B. Lalmi, H. Oughaddou, H. Enriquez, A. Kara, S. Vizzini, B. Ealet, and B. Aufray, Appl. Phys. Lett. **97**, 223109 (2010).

[9] P. D. Padova *et al.*, Appl. Phys. Lett. **96**, 261905 (2010).

[10] P. Vogt, P. De Padova, C. Quaresima, J. Avila, E. Frantzeskakis, M. C. Asensio, A. Resta, B. Ealet, and G. L. Lay, Phys. Rev. Lett. **108**, 155501 (2012).

[11] C.-L. Lin, R. Arafune, K. Kawahara, N. Tsukahara, E. Minamitani, Y. Kim, N. Takagi, and M. Kawai, Appl. Phys. Exp. **5**, 045802 (2012).

[12] C. C. Liu, W. Feng, and Y. Yao, Phys. Rev. Lett. **107**, 076802 (2011).

[13] M. Ezawa and N. Nagaosa, Phys. Rev. B **88**, 121401(R) (2013).

[14] M. Ezawa, Phys. Rev. B **87**, 155415 (2013).

[15] M. Ezawa, Eur. Phys. J. B **85**, 363 (2012).

[16] M. Ezawa, Phys. Rev. Lett. **114**, 056403 (2015).

[17] T. P. Kaloni, N. Singh, and U. Schwingenschlögl, Phys. Rev. B **89**, 035409 (2014).

[18] N. D. Drummond, V. Zólyomi, and V. I. Fal'Ko, Phys. Rev. B **85**, 075423 (2012).

[19] M. Ezawa, New J. Phys. **14**, 033003 (2012).

[20] I. Zutić, J. Fabian, and S. Das Sarma, Rev. Mod. Phys. **76**, 323 (2004).

[21] Y. Wang, J. Zheng, Z. Ni, R. Fei, Q. Liu, R. Quhe, C. Xu, J. Zhou, Z. Gao, and J. Lu, Nano **7**, 1250037 (2012).

[22] Y. Wang, R. Quhe, D. Yu, J. Li, and J. Lu, Chin. Phys. B **24**, 087201 (2015).

[23] W.-F. Tsai, C.-Y. Huang, T.-R. Chang, H. Lin, H.-T. Jeng, and A. Bansil, Nat. Commn. **4**, 1500 (2013).

[24] S. Rachel and M. Ezawa, Phys. Rev. B **89**, 195303 (2014).

[25] H. Pan, Z. Li, C.-C. Liu, G. Zhu, Z. Qiao, and Y. Yao, Phys. Rev. Lett. **112**, 106802 (2014).

[26] T. Yokoyama, Phys. Rev. B **87**, 241409(R) (2013).

[27] R. Saxena, A. Saha, and S. Rao, Phys. Rev. B **92**, 245412 (2015).

[28] L. Tao, E. Cinquanta, D. Chiappe, C. Grazianetti, M. Fanciulli, M. Dubey, A. Molle, and D. Akinwande, Nat. Nanotechnol. **10**, 227 (2015).

[29] J. Linder and T. Yokoyama, Phys. Rev. B **89**, 020504(R) (2014).

[30] G. C. Paul, S. Sarkar, and A. Saha, Phys. Rev. B **94**, 155453 (2016).

[31] S. Sarkar, A. Saha, and S. Gangadharaiah, arXiv:1609.0693.

[32] D. J. Thouless, Phys. Rev. B **27**, 6083 (1983).

[33] M. Büttiker, H. Thomas, and A. Prêtre, Z. Phys. B **94**, 133 (1994).

[34] P. W. Brouwer, Phys. Rev. B **58**, R10135 (1998).

[35] P. W. Brouwer, Phys. Rev. B **63**, 121303 (2001).

[36] M. Moskalets and M. Büttiker, Phys. Rev. B **66**, 205320 (2002).

[37] M. Moskalets and M. Büttiker, Phys. Rev. B **69**, 205316 (2004).

[38] A. Kundu, S. Rao, and A. Saha, Phys. Rev. B **83**, 165451 (2011).

[39] Q. Niu, Phys. Rev. Lett. **64**, 1812 (1990).

[40] I. L. Aleiner and A. V. Andreev, Phys. Rev. Lett. **81**, 1286 (1998).

[41] T. A. Shutenko, I. L. Aleiner, and B. L. Altshuler, Phys. Rev. B **61**, 10366 (2000).

[42] O. Entin-Wohlman, A. Aharony, and Y. Levinson, Phys. Rev. B **65**, 195411 (2002).

[43] O. Entin-Wohlman and A. Aharony, Phys. Rev. B **66**, 035329 (2002).

[44] R. Benjamin and C. Benjamin, Phys. Rev. B **69**, 085318 (2004).

[45] C. Benjamin and R. Citro, Phys. Rev. B **72**, 085340 (2005).

[46] S. Das and S. Rao, Phys. Rev. B **71**, 165333 (2005).

[47] S. Banerjee, A. Mukherjee, S. Rao, and A. Saha, Phys. Rev. B **75**, 153407 (2007).

[48] A. Agarwal and D. Sen, J. Phys.: Condens. Matter **19**, 046205 (2007).

[49] A. Agarwal and D. Sen, Phys. Rev. B **76**, 235316 (2007).

[50] R. P. Tiwari and M. Blaauboer, Appl. Phys. Lett. **97**, 243112 (2010).

[51] R. Zhu and H. Chen, Appl. Phys. Lett. **95**, 122111 (2009).

[52] J. Splettstoesser, M. Governale, and J. König, Phys. Rev. B **77**, 195320 (2008).

[53] S. Rojek, M. Governale, and J. König, Phys. Status Solidi B **251**, 1912 (2014).

[54] M. Switkes, C. Marcus, K. Campman, and A. Gossard, Science **283**, 1905 (1999).

[55] P. J. Leek, M. R. Buitelaar, V. I. Talyanskii, C. G. Smith, D. Anderson, G. A. C. Jones, J. Wei, and D. H. Cobden, Phys. Rev. Lett. **95**, 256802 (2005).

[56] S. K. Watson, R. M. Potok, C. M. Marcus, and V. Umansky, Phys. Rev. Lett. **91**, 258301 (2003).

[57] M. R. Buitelaar, V. Kashcheyevs, P. J. Leek, V. I. Talyanskii, C. G. Smith, D. Anderson, G. A. C. Jones, J. Wei, and D. H. Cobden, Phys. Rev. Lett. **101**, 126803 (2008).

[58] F. Giazotto, P. Spathis, S. Roddaro, S. Biswas, F. Taddei, M. Governale, and L. Sorba, Nat. Phys. **7**, 857 (2011).

[59] M. Blumenthal, B. Kaestner, L. Li, S. Giblin, T. Janssen, M. Pepper, D. Anderson, G. Jones, and D. Ritchie, Nat. Phys. **3**, 343 (2007).

[60] E. Prada, P. San-Jose, and H. Schomerus, Phys. Rev. B **80**, 245414 (2009).

[61] M. Alos-Palop and M. Blaauboer, Phys. Rev. B **84**, 073402 (2011).

[62] R. Citro, F. Romeo, and N. Andrei, Phys. Rev. B **84**, 161301 (2011).

[63] M. Alos-Palop, R. P. Tiwari, and M. Blaauboer, New J. Phys. **14**, 113003 (2012).

[64] J. E. Avron, A. Elgart, G. M. Graf, and L. Sadun, Phys. Rev. Lett. **87**, 236601 (2001).

[65] Y. Levinson, O. Entin-Wohlman, and P. Wölfle, Physica A **302**, 335 (2001).

[66] A. Saha, D. Rainis, R. P. Tiwari, and D. Loss, Phys. Rev. B **90**, 035422 (2014).

[67] M. Gibertini, R. Fazio, M. Polini, and F. Taddei, Phys. Rev. B **88**, 140508(R) (2013).

[68] P. L. S. Lopes, P. Ghaemi, S. Ryu, and T. L. Hughes, Phys. Rev. B **94**, 235160 (2016).

[69] C. W. J. Beenakker, Phys. Rev. Lett. **97**, 067007 (2006).

[70] C. W. J. Beenakker, Rev. Mod. Phys. **80**, 1337 (2008).

[71] A. Kundu, S. Rao, and A. Saha, Phys. Rev. B **82**, 155441 (2010).

[72] J. Linder and A. Sudbø, Phys. Rev. Lett. **99**, 147001 (2007).

[73] S. Bhattacharjee and K. Sengupta, Phys. Rev. Lett. **97**, 217001 (2006).

[74] J. Cayssol, Phys. Rev. Lett. **100**, 147001 (2008).

[75] M. R. Sahu, P. Raychaudhuri, and A. Das, Phys. Rev. B **94**, 235451 (2016).

[76] H. B. Heersche, P. Jarillo-Herrero, J. B. Oostinga, L. M. K. Vandersypen, and A. F. Morpurgo, Nature (London) **446**, 56 (2007).

[77] J.-H. Choi, G.-H. Lee, S. Park, D. Jeong, J.-O. Lee, H.-S. Sim, Y.-J. Doh, and H.-J. Lee, Nat. Commun. **4**, 2525 (2013).

[78] V. E. Calado, S. Goswami, G. Nanda, M. Diez, A. R. Akhmerov, K. Watanabe, T. Taniguchi, T. M. Klapwijk, and L. M. K. Vandersypen, Nat. Nanotechnol. **10**, 761 (2015).